Study Concerning Contact Strain and Stresses in Radial-Axial Bearings

Ionut Geonea(✉), Ilie Dumitru, Alexandru Oprica, and Nicoleta Gencărau

Faculty of Mechanics, University of Craiova, Craiova, Romania
ionut.geonea@edu.ucv.ro

Abstract. In this paper we will present theoretical notions, supplemented with studies performed with the finite element method on the distribution of forces in the axial radial ball bearings, as well as the distribution of deformations and stresses on the raceways and rolling bodies of the bearings. The theoretical model for determining contact stresses and strains is based on the elliptical contact theory developed by Hertz. The 3D model of a radial axial bearing type 6204 was constructed and analysed with numerical methods. The purpose of the numerical simulation is to determine the distribution of stresses and contact deformations between the rolling bodies and the bearing rings.

Keywords: bearing · mechanical stress · strain · FEA

1 Introduction

Research on determining the contact stresses (Hertzian) in bearings is presented in numerous studies, being considered groove ball bearing [1], large diameter ball bearing [2]. There are studies in which ANSYS finite element analysis software is used for ball bearing contact analysis [3]. Much more complex studies are also being conducted, which involve determining the dependencies between Hertz stress-life exponent, ball-race conformity, and ball bearing life [4], or methods to select a ball bearing and determine its actual reliability. [5]. Studies are also performed on the experimental determination of the friction moment in the bearings [5].

When the friction torques operate, in certain situations, the surfaces of the coupling bodies come into direct contact, and under external load, in the contact area, on the surfaces and in the depths, a state of local stresses and deformations develops.

Under the action of forces on the bodies in relative motion, the surfaces of the bodies deform, resulting in elliptical contact surfaces, at point contact, and in the form of a rectangular band, at linear contact, unanimously accepted by specialists. Determining body contact involves solving the following problems:

- Contact geometry of the common contact surface (contact ellipse half-axes or contact band half-width);
- Distribution of stresses in the contact area (on the contact surface and near the contact area);

© The Author(s) 2023
I. Dumitru et al. (Eds.): ICOME 2022, AHE 15, pp. 313–321, 2023.
https://doi.org/10.2991/978-94-6463-152-4_35

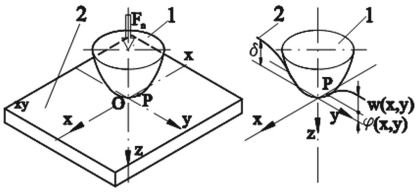

Fig. 1. Contact between a curved rigid body 1 and an elastic flat body 2.

- Total contact deformation (relative proximity of bodies).

The calculation of contact stresses and strains involves solving the equations in the theory of elasticity, without considering the friction of bodies.

The first theoretical research on contact theory was done by Rudolph Hertz, which is why contact theory is also called Hertz's theory. Hertz solved the equations of the linear theory of elasticity by introducing the following simplifying hypotheses: bodies are elastic, homogeneous and isotropic; stresses are linear deformation functions (physical linearity hypothesis); stresses are functions of position, deformation and temperature, but not of their gradient (local dependence hypothesis); body surfaces are smooth; the co-contact surface is small compared to the dimensions of the bodies and is considered flat.

By introducing the assumptions of smooth surfaces and neglecting the friction on the bodies in contact, only normal stress is transmitted.

The paper is structured in four parts. After the introductory part, there are theoretical aspects regarding the integral contact equation presented, then theoretical aspects regarding the determination of deformations and mechanical contact stresses are discussed. In the last part are presented aspects regarding the analysis with finite elements in ANSYS of deformations and stresses, based on a case study, performed on an axial radial bearing type SKF 6204.

2 The Integral Equation of Contact

The contact between a rigid curved body 1 and an elastic plane body 2 is considered, the contact being theoretically made at a point (Fig. 1, a).

Under the action of the external force F_n, which acts according to the common normal, the elastic body 2 deforms elastically, allowing the body 1 to penetrate the elastic half-space of the body 2 with a quantity δ (Fig. 1, b).

Let be a current point on the common contact surface of the two bodies, P (x, y), for which it is denoted by:

– φ (x, y) - the dimension of the point P with respect to the initial point of contact of the rigid body;
– w (x, y) - elastic displacement of the boundary of the elastic half-space corresponding to the point P (x, y).

The elastic displacement w (x, y) at the point of contact (z = 0) for a unit load, when the concentrated load is normal, established by Boussinesq, is given by the relation:

$$w = \frac{1-\nu^2}{\pi \cdot E} \cdot \frac{1}{\sqrt{x^2+y^2}} \tag{1}$$

And for a certain point of the contact surface (x'y'), for the pressure on the contact area, p_z, the elastic displacement will be:

$$w(x,y) = \frac{1-\nu^2}{\pi \cdot E} \iint_A \frac{p\left(x',y'\right)}{\sqrt{\left(x-x'\right)^2+\left(y-y'\right)^2}} dA \tag{2}$$

If both bodies are elastic, the integral equation of elastic contact displacements will be:

$$w(x,y) = w_1(x,y) + w_2(x,y) =$$
$$\frac{1}{\pi}\left(\frac{1-\nu_1^2}{E_1} + \frac{1-\nu_2^2}{E_2}\right) \iint_A \frac{p\left(x',y'\right)}{\sqrt{\left(x-x'\right)^2+\left(y-y'\right)^2}} dA \tag{3}$$

Taking into account the above relations, we obtain Eq. (4), which is the integral equation of contact. This integral equation allows to determine the pressure distribution, p_z (x, y), on the contact area of two bodies. The integral contact equation has many applications in technology: gears, bearings, mechanical speed variators, rolling stock, etc.

$$\frac{1}{\pi}\left(\frac{1-\nu_1^2}{E_1} + \frac{1-\nu_2^2}{E_2}\right) \iint_A \frac{p\left(x',y'\right)}{\sqrt{\left(x-x'\right)^2+\left(y-y'\right)^2}} dA = \delta - \frac{1}{2}\left(\frac{x^2}{R_x} + \frac{y^2}{R_y}\right) \tag{4}$$

where R_x and R_y are the equivalent radii of curvature in the main directions x and y.

3 Deformations and Contact Stresses

For point contact, the common contact surface has an elliptical shape with axes a and b (unknown), on which the pressure distribution, p_z (x, y), is considered to be ellipsoidal (Fig. 2), this hypothesis of distribution will be verified later.

So, for a certain point, with the coordinates (x, y) belonging to the elliptical contact surface, the pressure is:

$$p((x,y)) = p_0\sqrt{1-\frac{x^2}{a^2}-\frac{y^2}{b^2}} \tag{5}$$

where p_0 is the maximum nominal pressure reached in the centre of the ellipse with the value:

$$p_0 = \frac{3 \cdot F_n}{2 \cdot \pi \cdot a \cdot b} \tag{6}$$

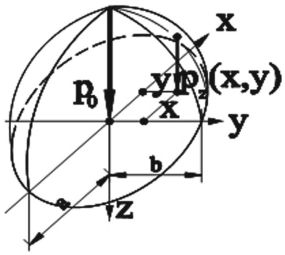

Fig. 2. The shape of the contact surface and the pressure distribution at the point contact.

Substituting the pressure in the integral contact equation with that given by relations (5) and (6) results in the semiaxes of the contact ellipse, a and b, which are given by the relations:

$$a = \sqrt[3]{\frac{3F_n}{\sum \rho} \cdot \frac{E(k^*)}{\pi \cdot (1-k^*)} \cdot \left(\frac{1-\nu_1^2}{E_1} + \frac{1-\nu_2^2}{E_2}\right)}$$

$$b = \sqrt[3]{\frac{3F_n}{\sum \rho} \cdot \frac{E(k^*) \cdot \sqrt{1-(k^*)^2}}{\pi} \cdot \left(\frac{1-\nu_1^2}{E_1} + \frac{1-\nu_2^2}{E_2}\right)} \tag{7}$$

where E (k *) is the complete elliptic integral with modulus k *, of the second case.

$$E(k^*) = \int_0^{\frac{\pi}{2}} \sqrt{1 - k^* \sin^2 \phi}\, d\phi \tag{8}$$

where k * is the eccentricity of the contact ellipse.

$$k^* = \sqrt{1 - \frac{b^2}{a^2}} \cong 1,0339 \cdot \left(\frac{R_x}{R_y}\right)^{0,636} \tag{9}$$

where:

$$\frac{1}{R_x} = \pm\frac{1}{R_{1x}} \pm \frac{1}{R_{2x}},\ \frac{1}{R_y} = \pm\frac{1}{R_{1y}} \pm \frac{1}{R_{2y}} \tag{10}$$

Relationships (7) can be written as:

$$a = a^* \sqrt[3]{\frac{3F_n}{E' \cdot \sum \rho}} \quad \bigcup a^* = \sqrt[3]{\frac{2 \cdot E(k^*)}{\pi \cdot \left[1-(k^*)^2\right]}}$$

$$\mathrm{b} = \mathrm{b}^* \sqrt[3]{\frac{3\mathrm{F_n}}{\mathrm{E}' \cdot \sum \rho}} \quad \bigcup \mathrm{b}^* = \sqrt[3]{\frac{2 \cdot \sqrt{1-(\mathrm{k}^*)^2} \cdot \mathrm{E}(\mathrm{k}^*)}{\pi}} \tag{11}$$

where $\frac{1}{E'} = \frac{1}{2}\left(\frac{1-\nu_1^2}{E_1} + \frac{1-\nu_2^2}{E_2}\right)$.

Table 1. Mechanical characteristics of bearing steel

Property	Value	Unit
Density	7850	kg· m^3
Young's Modulus	2.12 ·1011	Pa
Poisson's Ratio	0.29	-
Bulk Modulus	$1.6825 \cdot 10^{11}$	Pa
Shear Modulus	$8.2171 \cdot 10^{10}$	Pa
Tensile Yield Strength	$7{,}61 \cdot 10^{8}$	Pa
Tensile Ultimate Strength	$1.07 \cdot 10^{9}$	Pa

The relative proximity between the two bodies in contact (penetration) is calculated by the relation:

$$\delta = \delta^* \cdot \sqrt[3]{\left[\frac{3F_n}{E' \cdot \sum \rho}\right]^2} \cdot \frac{\sum \rho}{2}, \bigcup \delta^* = \frac{2 \cdot F(k^*)}{\pi} \cdot \sqrt[3]{\frac{\pi \cdot (1 - k^*)^2}{2 \cdot E(k^*)}} \tag{12}$$

where F (k *) is the elliptic integral with modulus k *.

4 Finite Element Analysis of Strain and Contact Stresses

To carry out these studies, we developed the assembly model of a radial-axial bearing SKF 6204, using Solid Works software. The CAD model includes the outer and inner rings, the cage as well as the rolling bodies, as shown in Fig. 3.

The different regime of the stresses, as well as the particularly complex character of the deterioration phenomena led to the establishment of some direct links between the mechanical properties and the quality of the materials used in the construction of the bearings. Experimental studies have established that in order to assess the quality of bearing steel, the following characteristics must be taken into account: durability and stress on contact fatigue, hardness at ambient temperature and high temperatures, coefficient of expansion, toughness, corrosion resistance, etc.

For normal uses and conditions, only the first two characteristics are important, the others becoming important only for special purpose bearings.

Steels with a high carbon content of 1% and a chromium content of 1.5% were selected for the bearing rings and rolling bodies. For the components of the bearing, we specified a steel used in the construction of bearings, type RUL1V. The characteristics of this material are specified in Table 1.

We performed the meshing with hexahedron finite elements. This aspect is shown in Fig. 3.

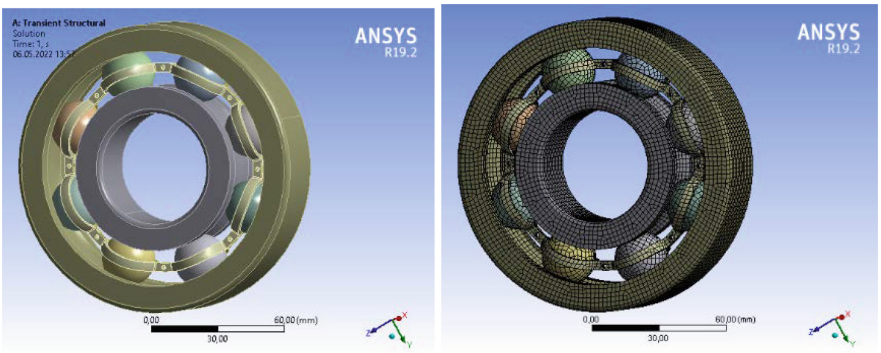

Fig. 3. CAD model of the bearing and finite element discretization.

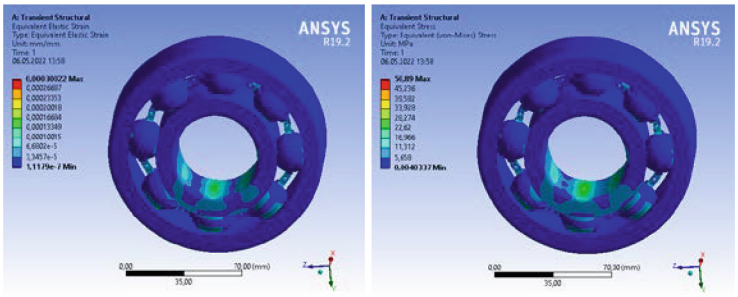

Fig. 4. Distribution for equivalent strain and (von Mises) Stress.

We performed a finite element analysis using the ANSYS Workbench program. As contour conditions we specified a contact pressure of 10 MPa, which acts on the inner ring, while the outer ring is fixed. The contact between the rolling bodies and the rings is of the "Bonded" type. In Fig. 4, the results obtained for this simulation are presented. According to Fig. 4, it is observed that the maximum value of the equivalent von Mises stress is 50.89 MPa, which appears with the most loaded rolling body, ie the ball in the lower position on the vertical direction. The maximum specific deformation is 0.00030022 mm/mm.

In order to visualize the distribution of von Mises stresses and specific deformations on the component elements, we hide the rings in the first phase, in order to visualize the rolling bodies. Thus in Fig. 5, shows the results obtained on the three rolling bodies that take over the load from the bearing.

It is found that on the bearing rings the shape of the von Mises stress distribution and the specific deformations is elliptical.

In the case of a radial ball bearing, of the SKF 6204 type, the dependence between the equivalent von Mises stresses, the equivalent specific deformations, is shown in Fig. 8. It is found that these dependencies are linear.

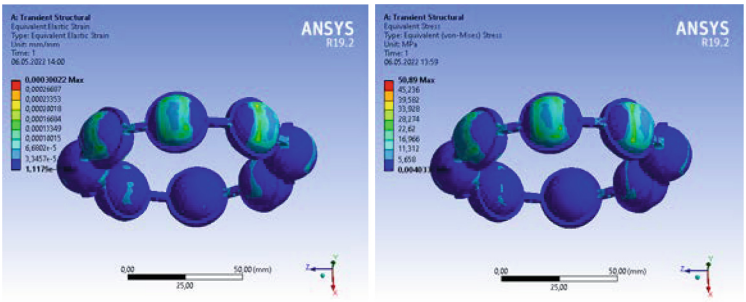

Fig. 5. Equivalent strain and (von Mises) Stress for rolling bodies.

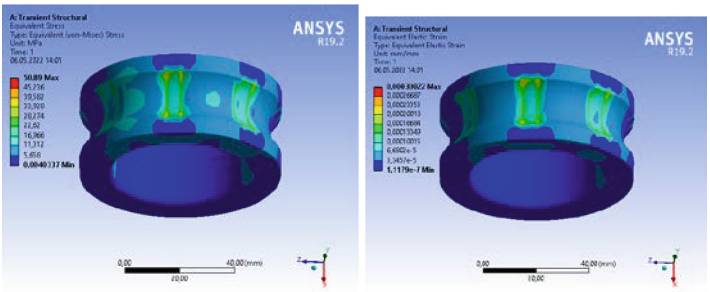

Fig. 6. Equivalent strain and (von Mises) Stress for the inner ring.

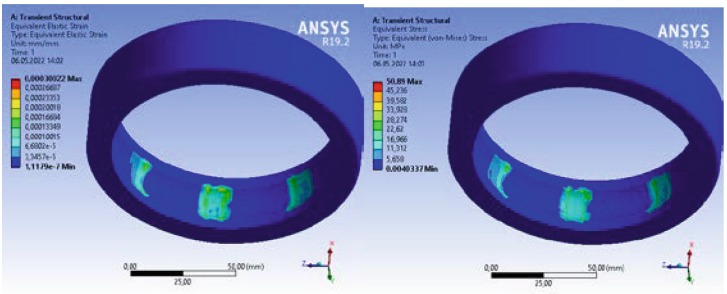

Fig. 7. Equivalent strain and (von Mises) Stress for the outer ring.

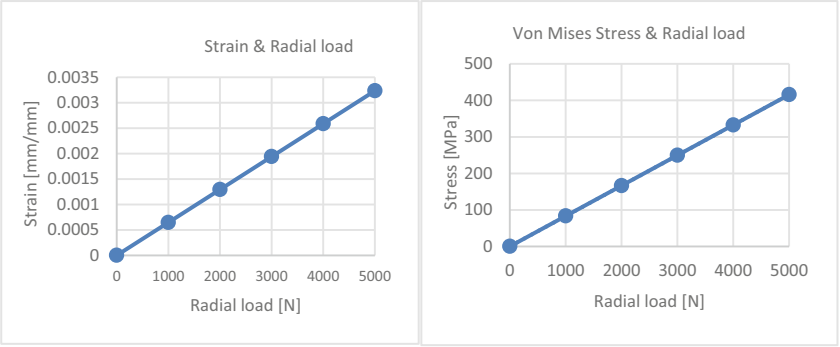

Fig. 8. Stress-strain & radial load dependence for SKF 6204 bearing.

5 Conclusions

In this paper we presented theoretical aspects regarding the calculation of the contact deformations and the stresses that appear at the contact between the rolling bodies of the bearings and the rings. We considered as a case study, the SKF bearing type 6204. We obtained by numerical simulation in ANSYS the distribution of contact stresses as well as the specific deformations. According to Fig. 4, 5, 6 and 7, it is observed that this distribution is an elliptical one. These results were obtained for the hypothesis in which we considered deformable both the rolling bodies and the rings.

References

1. Anoopnath, P. R., Babu, V. S., Vishwanath, A. K.: Hertz contact stress of deep groove ball bearing. Materials today: proceedings, 5(2), 3283-3288, (2018).
2. Pandiyarajan, R., Starvin, M. S., Ganesh, K. C.: Contact stress distribution of large diameter ball bearing using Hertzian elliptical contact theory. Procedia Eng., 38, 264-269, (2012).
3. Zhaoping, T., Jianping, S.: The contact analysis for deep groove ball bearing based on ANSYS. Procedia Engineering, 23, 423-428, (2011).
4. Zaretsky, E. V., Poplawski, J. V., & Root, L. E.: Relation between Hertz stress-life exponent, ball-race conformity, and ball bearing life. Tribology transactions, 51(2), 150-159, (2008).
5. Villa-Covarrubias, B., Piña-Monarrez, M. R., Barraza-Contreras, J. M., Baro-Tijerina, M.: Stress-based Weibull method to select a ball bearing and determine its actual reliability. Applied Sciences, 10(22), 8100, (2020).
6. Geonea, I., Dumitru, N., Dumitru, I.: Experimental and theoretical study of friction torque from radial ball bearings. In IOP Conference Series: Materials Science and Engineering (Vol. 252, No. 1, p. 012048). IOP Publishing. (2017).

Open Access This chapter is licensed under the terms of the Creative Commons Attribution-NonCommercial 4.0 International License (http://creativecommons.org/licenses/by-nc/4.0/), which permits any noncommercial use, sharing, adaptation, distribution and reproduction in any medium or format, as long as you give appropriate credit to the original author(s) and the source, provide a link to the Creative Commons license and indicate if changes were made.

The images or other third party material in this chapter are included in the chapter's Creative Commons license, unless indicated otherwise in a credit line to the material. If material is not included in the chapter's Creative Commons license and your intended use is not permitted by statutory regulation or exceeds the permitted use, you will need to obtain permission directly from the copyright holder.